KSME

Springer

Journal of Mechanical Science and Technology 34 (8) 2020

Original Article
DOI 10.1007/s12206-020-0718-y

Keywords:
· Energy density
· Laser power
· Scan speed
· Selective laser melting (SLM)
· Small punch test
· Strength
· 17-4PH

Correspondence to:
Jong Min Yu
lig01@nate.com

Citation:
Lee, H. J., Dao, V. H., Ma, Y. W., Yu, J. M., Yoon, K. B. (2020). Effects of process parameters on the high temperature strength of 17-4PH stainless steel produced by selective laser melting. Journal of Mechanical Science and Technology 34 (8) (2020) 3261~3272.
http://doi.org/10.1007/s12206-020-0718-y

Received March 14th, 2020
Revised May 6th, 2020
Accepted May 19th, 2020

† Recommended by Editor
Chongdu Cho

Effects of process parameters on the high temperature strength of 17-4PH stainless steel produced by selective laser melting

Ho Jun Lee[1], Van Hung Dao[1], Young Wha Ma[2], Jong Min Yu[1] and Kee Bong Yoon[1]

[1]Department of Mechanical Engineering, Chung-Ang University, 84 Heukseok-ro, Dongjak-Gu, Seoul 06974, Korea, [2]R&D Institute, Doosan Heavy Industries & Construction Co., Changwon, Korea

Abstract In this study, the effects of process parameters on the high temperature strength of 17-4PH stainless steel manufactured by selective laser melting (SLM) were investigated. Nine rectangular block specimens were fabricated with various process parameters. Small punch (SP) tests were conducted at 425 °C four times for each rectangular block specimens. The average maximum SP loads were measured from the tests. The fracture surfaces of SP-tested specimens were also examined. Un-melted powder was observed on the fracture surface of the specimen with the lowest average maximum SP load value, which could give rise to local cracking. Analysis of the microstructures showed that the retained austenite and amount of pore defects were the main factors that could affect SP test results. Regression surface methodology (RSM) models was applied to predict the maximum strength as a function of laser scan speed and energy density. Results showed that the energy density level of 64.29 J/mm^3 and a scan speed higher than 1884 mm/s are recommended for fabricating SLM parts in the shortest time without losing material strength and with minimum metallurgical defects.

1. Introduction

Among various additive manufacturing (AM) technologies, selective laser melting (SLM) has been considered as a suitable technique in rapid prototyping to manufacture fully dense metal parts from pre-alloyed material such as 17-4PH, AlSi12, Ti4Al4V, and AISI 316L stainless steel [1-4]. Wide usage of the SLM is because of many advantages such as low cost, high laser energy density, fewer steps in the production process, and design freedom [5]. Moreover, the products manufactured using SLM showed higher strength, better elongation, and improved corrosion resistance [3, 6-8]. The quality of SLM parts primarily depends on microstructural features. The microstructure is affected by SLM processing parameters such as hatching distance, scan speed, laser power [9], or the thermal history experienced during processing [10].

17-4PH precipitation-hardened stainless steel is attractive due to superior mechanical properties attributed to the precipitation of copper-rich spherical particles in the martensite matrix combined with moderate weldability, corrosion resistance, and oxidation resistance [11, 12]. The 17-4PH stainless steel is widely used in aerospace, chemical, and petrochemical industries. This material was used for fabricating turbine blade component which required the high strength at high working temperature. Recently, several studies regarding the microstructure and mechanical behavior such as strength, fatigue and fracture for 17-4PH precipitation-hardened steel processed by SLM have been conducted [1, 12, 13]. These studies elucidated the unique characteristics of SLM parts, including defects (pores, un-melted regions, and lack of fusion), microstructure features, and anisotropic tensile and fatigue behavior with different building directions. Ref. [14] reported the effects of building orientation and heat treatment on the fatigue behavior of SLM 17-4PH stainless steel, which demonstrated a lower elongation to failure for vertically built specimens. Heat treatment was found to be essential for enhancing tensile strength. In addition, the effect of manufacturing direction was also [15]. A similar effect

on fracture toughness and fatigue resistance was also observed for SLM Ti-6Al-4V material [16]. Furthermore, few studies have focused on the effect of processing parameters on the final parts of 17-4PH stainless steel manufactured by SLM. The effects of scan velocity, slice thickness, and hatching distance on the density, characteristics of the pore and micro-hardness have been reported [17]. The effects of energy density on the microstructural characterization and porosity formation of SLM 17-4PH stainless steel parts were investigated [18]. The results showed that the austenitic grain diameter was increased with a decrease in the scan speed at a constant laser power. It also showed that the pores were smaller and more circular with both a high laser power and a high scan speed. The δ-ferrite structure was fine at a low laser power and coarse at a high laser power [19]. Ponnusamy et al. [20] reported that 270 W laser power, vertical orientation, 30 μm layer thickness, and 6 mm defocus distance are required to achieve maximum hardness and compressive strength with least porosity for SLM 17-4PH stainless steel.

For experimental data reduction, several studies employed experimental design methodology and statistical regression analysis. Read et al. [3] used a statistical experimental design to optimize the process parameters for minimizing the porosity of SLM AlSi10Mg material. Casalino et al. [2] conducted an experimental investigation and a successive statistical optimization of 18Ni300 maraging steel; a laser power larger than 90 W and a velocity smaller than 220 mm/s were recommended for the best part properties. Miranda et al. [9] investigated the effect of SLM processing parameters on the shear strength, hardness, and density in the vertical and horizontal directions of SLM 316L stainless steel.

In this study, the high temperature strength of 17-4PH stainless steel manufactured by selective laser melting (SLM) was investigated using small punch (SP) test method. The SP method has been traditionally used as a tool for assessing the mechanical properties with small amount of materials. The tests were conducted at 425 °C for nine block samples manufactured by SLM with various process parameters. The maximum SP load and fracture surface were compared. The microstructure of the 17-4PH stainless steel samples and correlation with specific properties were also assessed. A statistical experimental method was used to determine the high scan speed obtainable without losing the material strength and with little manufacturing defects.

2. Experimental procedures

2.1 Material and SLM manufacturing

17-4PH stainless steel powder commercially available from the SLM equipment manufacturer was used for building rectangular blocks. The average particle size was 10 to 45 μm, as shown in Fig. 1(a). The chemical composition of the powder provided from the supplier [21] is shown in Table 1.

Nine rectangular blocks (from A to I) with a dimension of 23×16×16.5 mm were fabricated as shown in Fig. 1(b) by an

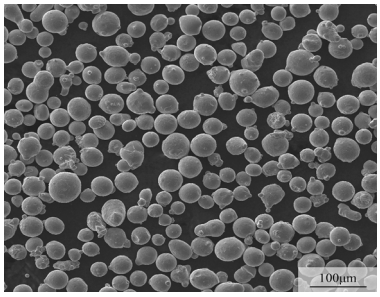

(a)

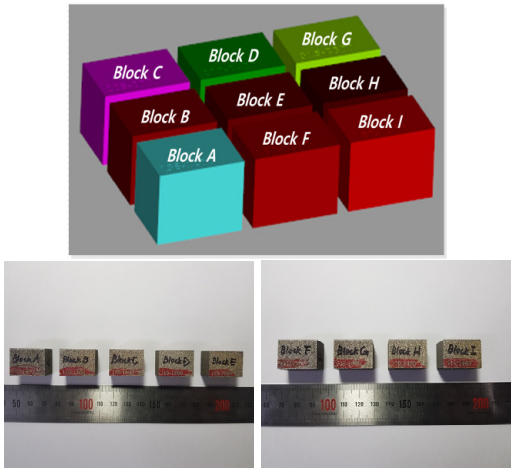

(b)

Fig. 1. (a) Morphology of the 17-4PH powder; (b) layout of block specimens during SLM fabrication (A to I blocks).

SLM (ProX 300 from 3D systems) machine. The laser beam with various laser power moved at a speed of 1200–2800 mm/s during manufacturing. The laser power was increased from 135 W to 315 W. The hatching distance was kept constant as 0.05 mm and the layer thickness as 0.04 mm, respectively. Then, the energy density values could be determined in the range from 45 to 75 J/mm^3 by using various combinations of scan speed and laser power. The detailed combinations of processing parameters are summarized in Table 2. For one set of blocks were manufactured under the condition of constant laser power with increasing scan speed. The other set of blocks were prepared under constant energy density condition.

Before the building process, the platform temperature was pre-heated at 250 °C to obtain the highest density of the manufactured block and to avoid surface defects such as balling. Argon gas was flowed to protect the manufactured blocks from oxidation and fume generated by melting the powder during the SLM fabrication. The laser beam was focused on the 17-4PH powder of the new layer and the rectangular block component was built through layer-by-layer addition as shown in Fig. 2(a) until the designed shape was completed. Fig. 2(b) shows that scanning was performed with a bi-directional pattern. The angle of the scanning direction between the consecutive layers was 90°.

Table 1. Chemical composition of the 17-4PH powder (wt%) [21].

Material	C	Mn	P	S	Si	Cr	Ni	Cu	Nb + Ta	O	Fe
17-4PH (SLM powder)	0.07	1.00	0.04	0.03	1.00	15.0–17.5	3.0–5.0	3.0–5.0	0.15–0.45	0.10	Bal.

Table 2. Process parameters and small punch test results.

Material	Block	Process parameters (SLM)					Small punch test results	
		Laser power (W)	Scan speed (mm/s)	Energy density (J/mm^3)	Hatching distance (μm)	Layer thickness (μm)	Maximum SP load (N)	Specimen thick. (mm)
17-4PH	A	180	1200	75.00	50	40	1007.722	0.499
	B	180	1400	64.29	50	40	1021.171	0.500
	C	180	1600	56.25	50	40	979.565	0.500
	D	180	1800	50.00	50	40	919.931	0.501
	E	180	2000	45.00	50	40	898.797	0.500
	F	135	1200	56.25	50	40	990.353	0.501
	G	225	2000	56.25	50	40	922.966	0.499
	H	270	2400	56.25	50	40	992.913	0.503
	I	315	2800	56.25	50	40	914.400	0.493

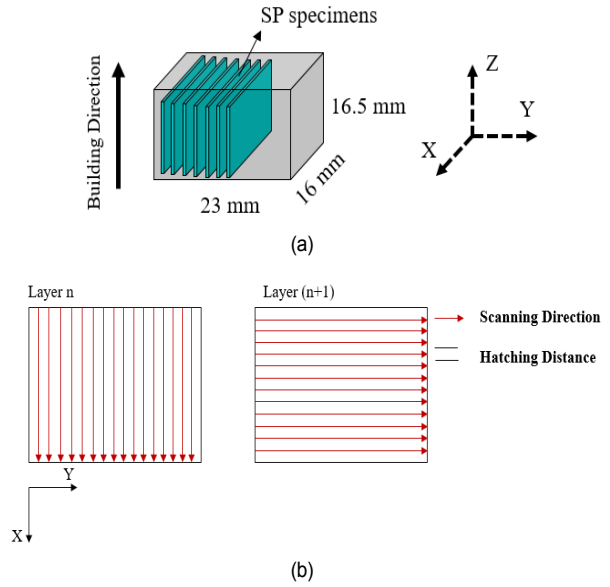

Fig. 2. (a) SLM-manufactured blocks showing the specimen machining directions for small punch (SP) test specimens; (b) schematics showing the scan strategy for planes accumulated in the building direction (scan direction rotated by 90° after each layer).

2.2 Small punch test and metallurgical investigation

The SP testing method is a miniaturized mechanical test technique developed in the 1980s [22, 23]. SP test is currently being standardized which covers the classical test for tensile property estimation and creep property evaluation [24]. The SP test has been performed for measuring tensile fracture characteristics [25, 26] and creep properties for different materials in a wide temperature range [27, 28]. Besides, this method has several advantages over the conventional full scale tests. The SP test specimens can be extracted from complex and component representative geometries.

The high temperature SP tests were repeated four times under the same conditions for each block, in this study. SP specimens were machined by wire cutting of each rectangular block. The size of each SP specimen was initially 10×10×0.6 mm. The SP specimens were polished on both sides to obtain flat and smooth surfaces by grinding with 800 grade SiC abrasive paper. The final thickness of the specimens was 0.5±0.007 mm. The final geometry of the specimen was 10×10×0.5 mm.

The jig for the SP test is shown in Fig. 3. The diameter of the loading ball was 2.38 mm. The lower die hole has 4 mm diameter. Edge of the hole was chamfered with corner radius of 0.2 mm. The SP test jig was in compliance with the European Code of Practice [24]. SP testing was conducted at 425 °C using an INSTRON Universal (E2-016) test machine with a 100 kN capacity. The load was applied to the specimen via the loading ball with a constant loading rate of 0.2 mm/min. During the test, the punch load and displacement data were automatically recorded in the form of plotted curves and displayed. The high temperature SP tests were repeated four times under the same conditions for each block.

The microstructure and fracture surface of the SP specimens in the XZ plane, as indicated in Fig. 2(a), were examined by light optical microscopy and scanning electron microscopy (SEM). Metallographic specimen was prepared as follows: the specimens were ground using silicon carbide papers with a grit size of 320–2400 and polished on a cloth with 0.6 and 0.1 μm diamond suspensions, and cleaned using an ultrasonic ma-

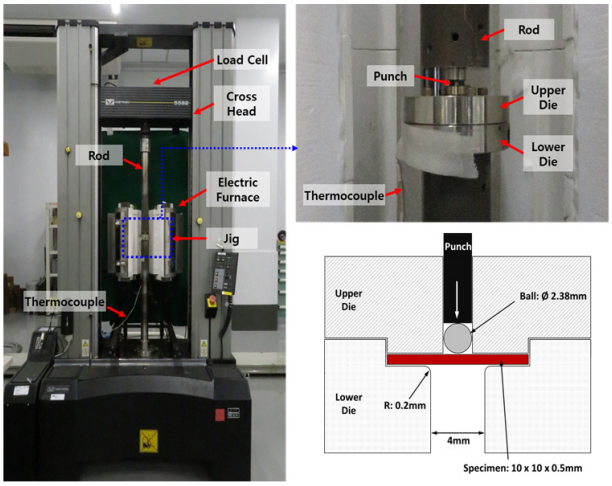

Fig. 3. Experimental SP equipment and SP test jig setup.

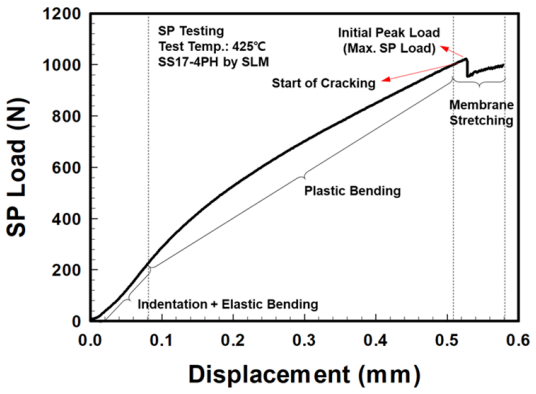

Fig. 4. SP test curve of SLM as-built 17-4PH stainless steel with identification of the different zones.

chine for 5 min in ethanol solution. Finally, they were etched with a solution of HNO_3, HCl, and glycerol. For phase identification of a constituent in the microstructure, X-ray diffraction (XRD) analysis was conducted with X-ray at 4°/min over a wide range of 2Θ = 30–100°, which could provide a general overview of the diffraction peaks.

2.3 Regression of the SP strength data using RSM

Response surface methodology (RSM) is a kind of regression used to optimize a process response (output variable) which may be influenced by several independent variables (input variables). The RSM aims to reduce the number of required experimental runs to generate statistically validated results and minimize the associated numerical noise. This technique was successfully employed for assessing the significance of the effect of SLM or selective laser sintering process variables on porosity fraction, crack density, and roughness of the manufactured products [3, 29, 30].

In this study, RSM was applied to predict the maximum SP load value achievable by using combinations of key SLM processing parameters. Usually, mechanical and microstructural analyses are necessary for determining the best processing conditions for the maximum strength. For the 17-4PH SLM blocks, RSM and microstructural analyses were performed together to determine optimal process parameters to obtain the maximum strength represented by the maximum SP load.

In RSM, mathematical models are applied for multiple regression analysis of the experimental data with the desired response as a function of selected variables. A second-order model can significantly improve the optimization process and obtain the equation coefficient when a first-order model suffers lack of fit due to effect of the interaction between the variables. A general second-order model is defined as shown in Eq. (1):

$$y = \beta_0 + \sum_{i=1}^{k} \beta_i x_i + \sum\sum_{i<j} \beta_{ij} x_i x_j + \sum_{i=1}^{k} \beta_{ii} x_i^2 + \varepsilon \quad (1)$$

where y is the response variable representing output data; x_i and x_j are independent variables of input data; β is the estimated regression constants; ε represents the noise or error observed in the response y. The maximum SP load was used as a response variable and the energy density and the scan speed were used as two independent variables. Then, the RSM analysis is useful to estimate the effect of two variables and their interactions in the SLM manufacturing process with the 17-4PH material.

3. Results and discussion

3.1 Maximum SP load measured by small punch tests

It was known that the SP load-displacement curves consist of four regions such as the initial period of elastic and plastic bending, membrane stretching, and cracking or thinning of the specimen leading to final failure [25, 31-33]. A typical SP load-displacement curve is shown in Fig. 4. The initial deformation called indentation and elastic bending occurs at the beginning section of the load-displacement plot. The displacement range of the indentation and elastic bending appeared to be approximately 0.01 mm, as shown in Fig. 5. Then, an extended phase of two permanent deformation modes, i.e, plastic bending and membrane stretching, occurred at the next stage of the curve until cracking failure occurred. The first peak load drop observed on the SP curve could be attributed to appearance of the first crack initiation on the SP surface, and the load at this point was defined as the maximum SP load as shown in Fig. 4. The average values of the maximum SP load were obtained from four test results are summarized in Table 2.

Fig. 5 shows four SP load-displacement curves in one graph for a SLM block, which were obtained with duplicated SP specimens manufactured under the same SLM manufacturing condition. For example, the first graph of Fig. 5(a) has four SP load-displacement curves for block A, measured with four specimens, all of which had manufactured by SLM under the same condition of scan speed (1200 mm/s), energy density

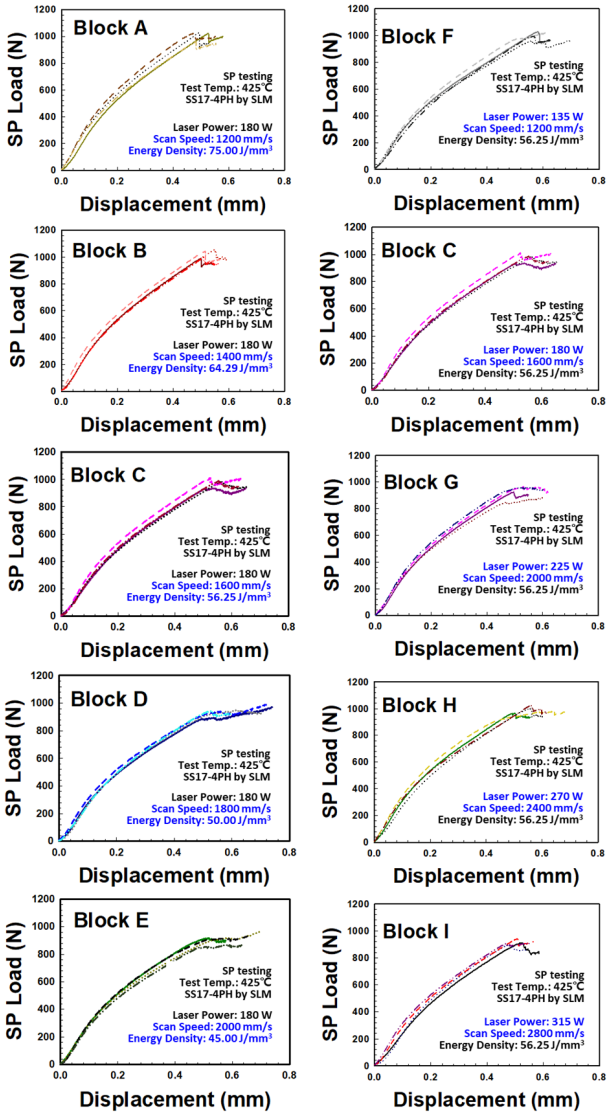

Fig. 5. Load vs. punch displacement curves during SP testing manufactured using SLM for 17-4PH stainless steel under various processing parameters: (a) for decreasing energy density; (b) for constant energy density.

(75.00 J/mm^3) and laser power (180 W). Therefore, characteristics of these four SP curves were quite similar as expected. Similarly, graphs for blocks B, C, D, and E are also shown in order in Fig. 5(a). For these blocks, the laser power was kept constant as 180 W. But, the scan speed was gradually increased to 1400, 1600, 1800 and 2000 mm/s. Since the scan speed was increased with the same laser power of 180 W, the energy density was decreased to 64.29, 56.25, 50.00 and 45.00 J/mm^3. In the Fig. 5(a), SP curves of block A and B showed clear initial peak load, respectively. The curves of block C, D and E had lower maximum SP loads and longer displacements before failure, comparing to block A and B. From the block A to E, the first peak load drop occurred at similar displacement of 0.5 mm. However, as the energy density of

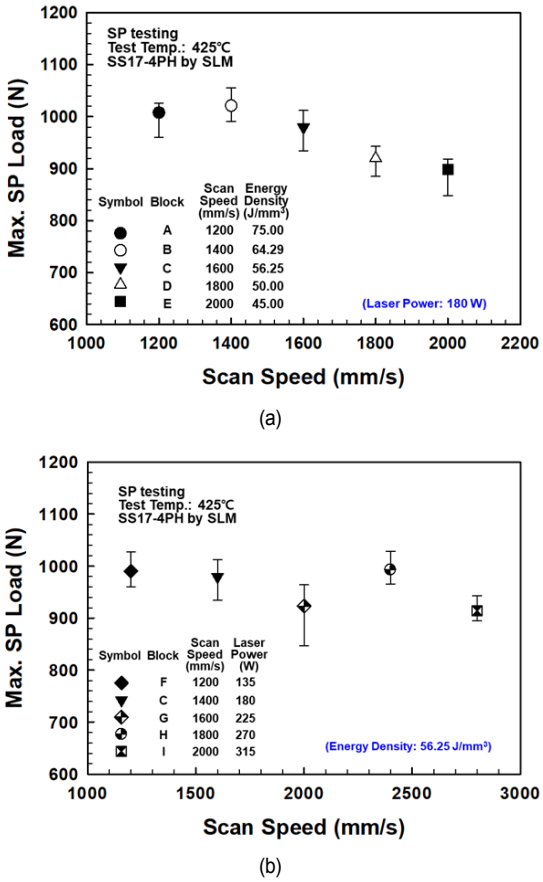

Fig. 6. Effect of SLM process parameters on the maximum SP load for each block with (a) decreasing energy density (increasing scan speed and constant laser power); (b) constant energy density (increasing laser power and scan speed).

the block specimen decreased, the displacement from the first peak-load drop to the fracture increased. Average values of the maximum SP load for all of these blocks with data scatter band are shown in Fig. 6(a) and Table 2.

Differently from Fig. 5(a) cases, in Fig. 5(b) the energy density was kept constant as 56.25 J/mm^3 for the blocks F, G, H, and I. To make these blocks have the same energy density of 56.25 J/mm^3, the laser power was also increased from 135 W to 315 W, as the scan speed increased from 1200 mm/s to 2800 mm/s. The obtained SP test curves are shown in Fig. 5(b). Similar to block A to E, block F to I also showed the first peak-load drop at the displacement in the range of 0.5-0.6 mm. For block F, G and H, the displacement after first peak-load drop until failure were in similar range of 0.1 mm. But block I showed shorter displacement after first peak-load drop. The measured average values of the maximum SP load are included in Fig. 6(b) and Table 2. The SLM manufacturing condition of block C having energy density value of 56.25 J/mm^3, can be included in this set of data between block F and block G for data trend analysis, as shown in Fig. 6(b).

Variation of the maximum SP load with increasing the scan speed is shown in Fig. 6(a). Since the laser power was con-

stant (180 W) during SLM manufacturing, increasing the scan speed means decreasing the energy density too. The maximum SP load was increased from 1007.7 N to 1021.2 N when the energy density was decreased from 75.00 J/mm^3 to 64.29 J/mm^3 (the scan speed was increased from 1200 to 1400 mm/s) for blocks A and B. When the energy density was decreased further, the maximum SP load value tended to decrease and reached the lowest value of 898.8 N when the energy density was 45.00 J/mm^3, corresponding to block E. The energy density of 64.29 J/mm^3 of block B showing the highest maximum SP load, could be considered as an optimal energy density level for SLM manufacturing with 17-4PH steel. Insufficient melting verified by un-melted powder and presence of pores in the microstructure was reported when the energy density was too low or when the scan speed was very high [18, 20]. These microstructural defects were observed in the blocks D and E. These defects could explain the decreased material strength represented by the maximum SP load.

In Fig. 6(b), the maximum SP load was compared among the blocks having the same energy density of 56.25 J/mm^3 with varying scan speed and laser power. Even though the maximum SP load values showed some fluctuations, it can be claimed that the strength was almost constant. The data did not show any systematic increase or systematic decrease. It seemed that the data scatter was caused by the randomness of the cracking mode.

3.2 Fractured surface and cracking shape of the SP specimens

The fractured SP specimen surfaces of two sets of the SP-tested specimens are shown in Fig. 7; Fig. 7(a) for the specimens if decreasing energy density and Fig. 7(b) for those with constant energy density. A fractured SP specimen surface usually showed crack initiation in a circular shape around the ball contact area growing from the outer surface of the specimen to the inner surface. In the plastic bending mode, the specimen was deformed due to the bending load generated by the ball contact with the specimen. During the membrane stretching mode, material stretching occurred in the annular region of the specimen surrounding the ball contact area where the extension of the specimen, thickness reduction, and crack initiation and growth occurred until the final failure. The fractured surfaces explained above were also reported previously [17].

In Fig. 7(a), blocks A, B and C showed circular shape cracks, from which the specimens must have normal strength property. On the other hand, block E showed a non-circular crack shape and several secondary cracks. The secondary cracks were started from the defects such as un-melted regions or pores existing in the specimen. Therefore, the cracking shapes on the specimen surface can explain the strength variation shown in Fig. 6(a). There was a considerable difference of the maximum SP load and the crack shape between the block B and E during the SP specimen deformation. The maximum SP load of

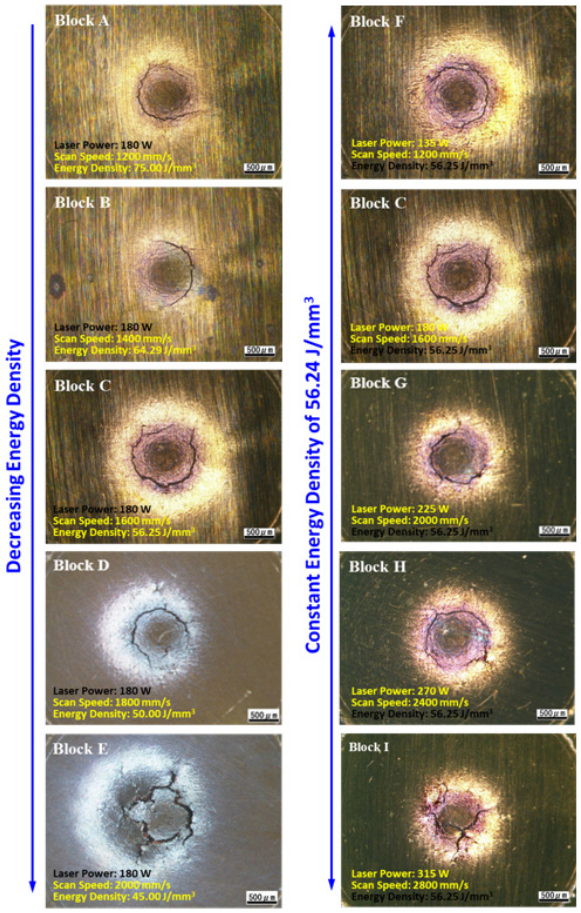

Fig. 7. Fracture surface observation of specimens after testing: (a) for decreasing energy density; (b) for constant energy density.

the block B which is the initial peak load, was much higher than the following peak loads after the first maximum load (Fig. 5(a)). On the other hand, the initial peak load of the block E was lower than the other peak loads after the first one. Furthermore, the punch displacement occurred after the maximum load point to the final fracture was much longer for block E (0.530 mm) than that of the block B (0.518 mm). This was due to the more ductile failure mode of the block E or due to contribution of the secondary cracks in the specimen E while the specimen A and B had a major single crack.

In Fig. 7(b), blocks F, C, G and H showed circular shape of cracks similar to blocks A, B and C. The block I showed a non-circular crack similar to the block E. From the cracking mode of block I, trend of the maximum SP load of block I in the Fig. 6(b) can be explained.

Fig. 8 shows comparison of the cracking regions on the SP specimen between the blocks B and E under high magnification (×1000, ×4000). Fig. 8(a) showed a circular crack of the block B having high strength. At the inside fracture surfaces of the major circular crack (B2) and the secondary crack (B1), no defects such as pores or un-melted powder were observed. Fig.

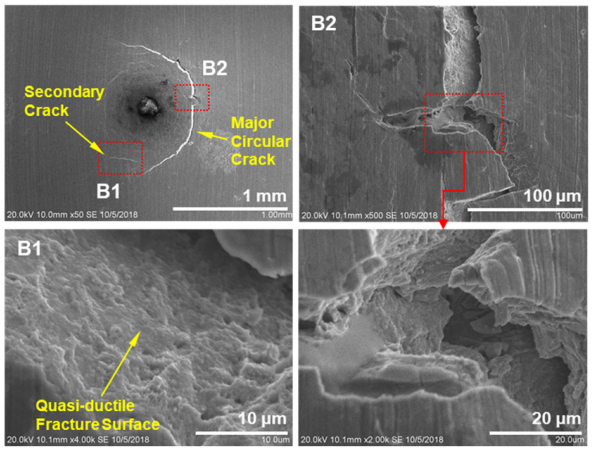

(a)

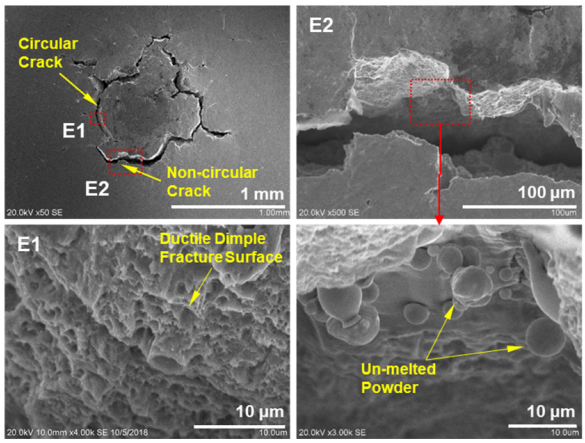

(b)

Fig. 8. Comparison of the fracture surface of the SP-tested: (a) block B; (b) block E specimens of SLM as-built 17-4PH stainless steel.

8(b) showed a non-circular crack of the block E having low strength. Inside of a circular shaped crack (E1) ductile fracture similar to that of B1, was observed. However, for a non-circular shaped crack (E2), un-melted powder (approximately 8–10 μm) was easily found. Since the energy density was not sufficient during manufacturing for block E, melting of the powder was not fully occurred. This kind of the internal defect can explain the difference in the maximum SP load between block B and E.

3.3 Observed phases and pore defects

3.3.1 Phase analyzed by XRD

The XRD spectra of the SLM 17-4PH stainless steel were measured and are shown in Fig. 9. Five randomly selected blocks (A, B, E, F, and G) with different process parameters were used for obtaining average analysis results. All of the specimens showed the presence of strong diffraction peaks corresponding to martensitic (α') and very low-intensity peaks, indicating a retained austenitic (γ) phase. Because of the rapid

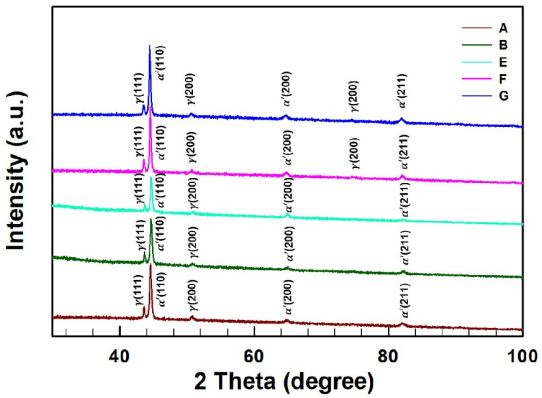

Fig. 9. XRD spectrum of the different block specimens of SLM as-built 17-4PH stainless steel.

solidification and cooling rates during the SLM process, martensitic formation are known to be dominate in the whole process. Generally, a fully martensitic structure can be obtained with conventional 17-4PH stainless steel [1] or after using a heat treatment method for SLM 17-4PH stainless steel [17]. When martensitic structure was increased, tensile strength and hardness of materials also increased. However, the presence of retained austenite in the microstructure can reduce martensitic transformation due to the refined austenitic grain size [14]. Consequently, the amount of retained austenite was increased primarily at grain boundaries where the martensitic phase cannot grow more [34]. This may significantly reduce tensile strength and hardness but may be beneficial for increasing strain hardening and elongation [1, 11]. Therefore, for the SLM 17-4PH steel, the retained austenite and its amount could have a significant effect on the SP tests of each block with varying processing parameters. Moreover, phase quantification of the retained austenite structure was tried and mentioned in the next section.

3.3.2 Pore defects observed by SEM

Fig. 10 shows optical micrographs in the XZ plane of the SLM blocks A~I of 17-4PH stainless steel. The circumferential area at the contact between the punch ball and the SP specimen was investigated before the SP testing. The martensitic structure of dark-colored region was observed in all blocks, which shows needle-like structure without well-defined grain boundaries. This martensitic structure contributes to high strength of the SLM manufactured 17-4PH parts [17]. The retained austenite was observed in a position interwoven with the martensitic structures, appeared as a white-colored region (see Fig. 10). Fig. 10(a) shows the microstructures of blocks A, B, D, and E manufactured under constant laser power and increasing scan speed conditions. In this figure, martensite, retained austenite and pore defects are indicated by arrows in all pictures. However, phase quantification of the martensite structure could not be measured due to pore defects appeared as the same color, as shown in Fig. 10. Therefore, phase quantifi-

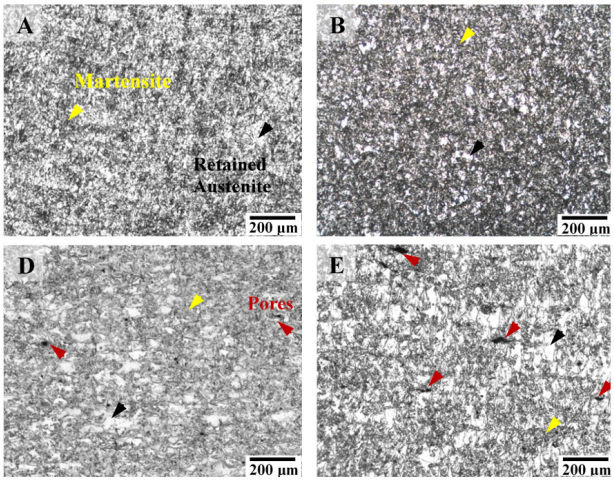

(a)

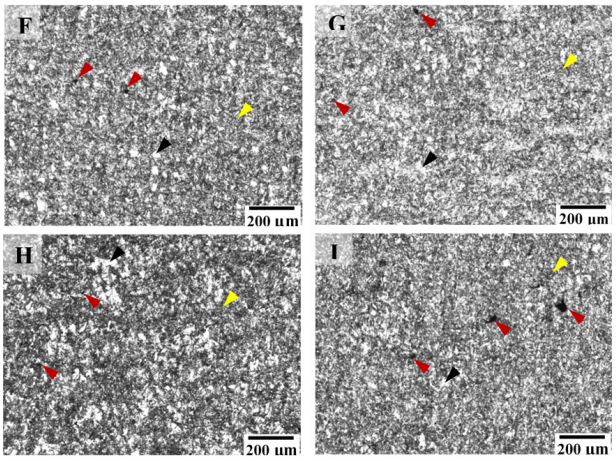

(b)

Fig. 10. Optical micrograph of the specimens of SLM as-built 17-4PH stainless steel: (a) blocks A, B, D, and E (constant laser power of 180 W); (b) blocks F, G, H, and I (constant energy density of 56.25 J/mm^3).

cation of the retained austenite structure appeared as a white-colored region could be identified. Since the block E was fabricated with the lowest energy density, it had the largest volume fraction of the retained austenite compared with the other blocks. The amount of volume fraction measured by image analysis method was 4.93 %, 8.95 %, and 17.22 % for block B, D, and E, respectively.

This result indicated that the retained austenite increased with decrease of the energy density, which was also observed by other studies [20, 35]. It can be claimed that one of the main factors that could significantly decrease the maximum SP load was the retained austenite and pore defects.

In addition, the pore defects in blocks A, B, D and E were examined. The amount of pore was greater in blocks D and E than that in blocks A and B. The size of the pores was also large for blocks D and E. For instances, the measured pore size (length × width) shown in Fig. 11 was 12.83×4.36 μm, 27.42×13.87 μm, and 57.56×25.83 μm for block B, D, and E, respectively. The measurement was conducted at a high magnification using SEM. The pore defects were significantly increased when the scan speed was increased and energy density was decreased [18]. The un-melted powder found at the fracture surface in a crack of block E (see Fig. 8) was actually in the pore defect after SLM manufacturing. Li et al. [36] also

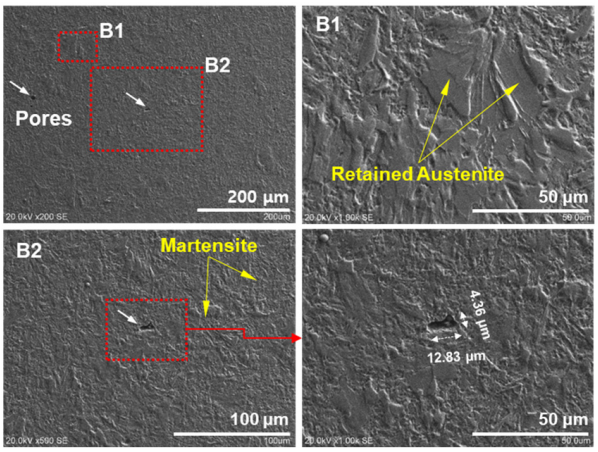

(a)

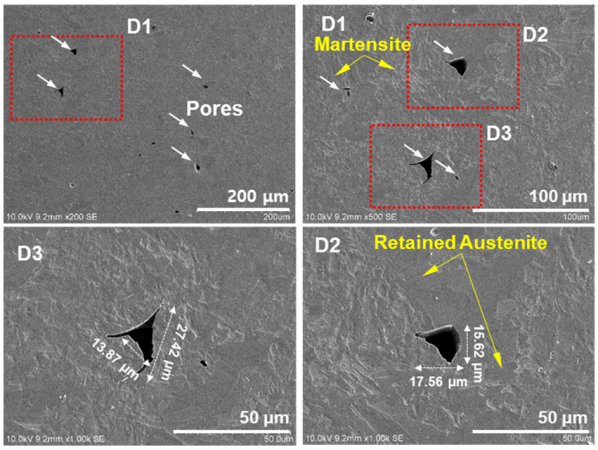

(b)

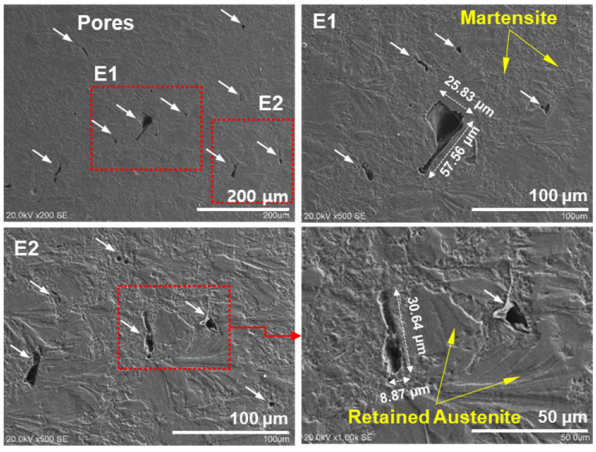

(c)

Fig. 11. SEM image of the SP specimens of SLM as-built17-4PH stainless steel before testing: (a) block B; (b) block D; (c) block E.

observed that when the scan speed was high and the laser power was constant, splashes of liquid balls had contributed to increased porosity and un-melted particles. This observed pore defects and un-melted powder, therefore, explains why the maximum SP load of block E was the lowest compared with those of other blocks.

The optical microstructures of blocks F, G, H, and I were also investigated, as shown in Fig. 10(b). Since the energy density was maintained at 56.25 J/mm^3 during SLM manufacturing, volume fraction of the retained austenite was not much different for all blocks. The amount of pore defects also did not show much difference. The block I showed some more defects. If the scan speed is increased exceeding the recommended limit while the energy density value is not sufficiently high, certain types of defects such as pores and un-melted region could be formed, reducing the strength. Therefore, the maximum SP load of block I was low compare to the other blocks which have same energy density.

3.4 Maximum SP strength predicted by RSM model

A regression equation was determined using the RSM model with the data of the nine blocks shown in Table 2. A three-factor interaction model was used to fit the data as follows:

$$P_{SP} = -3.003\times10^{3} - 3.130\times10^{-1}V - 3.640E + 8.382\times10^{3}a + 5.419\times10^{-3}VE \quad (2)$$

where P_{SP} is the maximum SP load (N), V is the scan speed (mm/s), E is the energy density (J/mm^3), and a is the SP specimen thickness (mm). Eq. (2) shows the independent and interactive relationship of V, E, a, and VE for the maximum SP load (P_{SP}). The energy density (E), SP specimen thickness (a), and interaction between scan speed and energy density parameters are the main factors that could affect the maximum SP load. The R^2 value, a measure for accuracy of the regression model fit, was 0.872, which indicated the model was adequate and supported that the predicted values were statistically similar to the measured values of the maximum SP load, as shown in Fig. 12. Consequently, the predicted model of Eq. (2) can be employed. Thickness of the SP specimen should be 0.5 mm according to the CEN standard [24]. The effect of specimen thickness to the maximum SP load is straightforward. Also, the range of the input variable, a, in Table 2 has a quite narrow range from 0.493 to 0.503 mm. The first order term of a, 8.382x10^3a, can have almost constant value of 4192 (4132~4216). The Eq. (2) can be rewritten as follows:

$$P_{SP} = 1.189\times10^{3} - 3.130\times10^{-1}V - 3.640E + 5.419\times10^{-3}VE \quad (3)$$

Fig. 13 shows the relationship between the scan speed, V, and energy density, E obtained by the RSM model. The maxi-

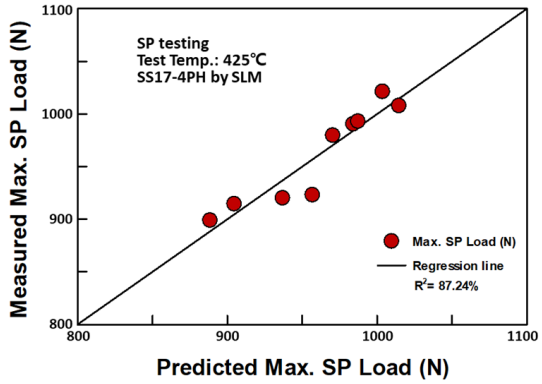

Fig. 12. Comparison between predicted and measured results for the maximum SP load of SLM as-built 17-4PH stainless steel.

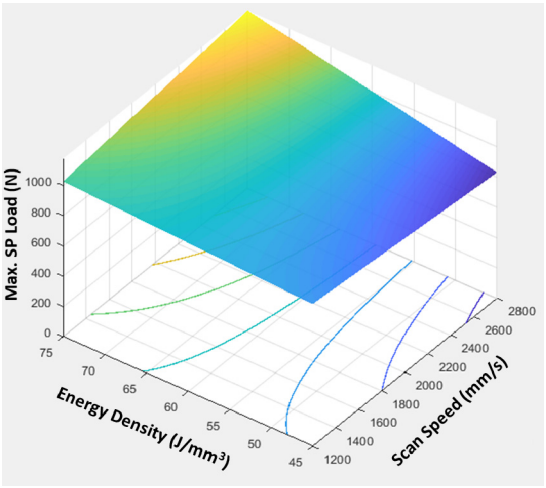

(a)

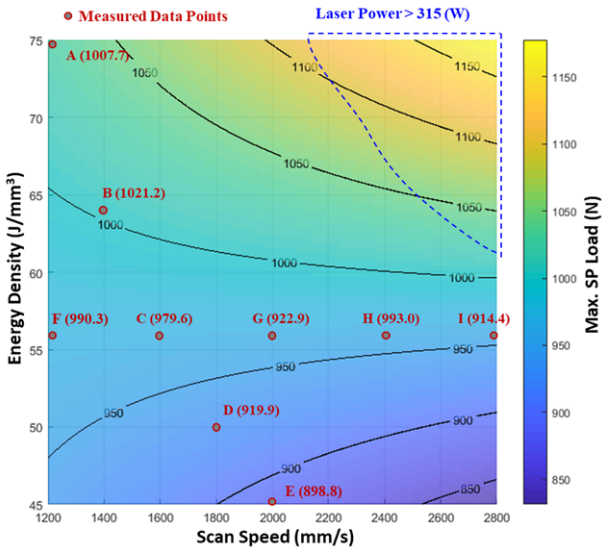

(b)

Fig. 13. Predicted maximum SP load versus scan speed and energy density for SLM built 17-4PH stainless steel: (a) surface plot; (b) contour plot with the measured data points.

mum SP load was increased when the energy density and scan speed were increased. The scan speed and energy density have a close correlation with the laser power. The relationship among these parameters is shown in Eq. (4):

$$E = \frac{p}{V \times d \times e} \tag{4}$$

where p is the laser power (W), V is the scan speed (mm/s), E is the energy density (J/mm^3), d is the hatching distance (mm), and e is the layer thickness (mm). According to Eq. (4), the energy density at the powder surface will be increased when the laser power is increased, when the scan speed is decreased and when hatching distance and layer thickness becomes smaller. For manufacturing the 17-4PH blocks, hatching distance and layer thickness were kept constant. Eq. (4) indicates that the laser power is a function of $E \times V$. Then, the 4th term in Eq. (2) can be considered as a term representing the laser power.

The laser power and scan speed can be controlled individually to determine energy input. Results shown in Fig. 13(a) indicates that the maximum SP load could be increased by increasing the energy density i.e, by increasing laser power and decreasing scan speed. Similar recommendations were made in previous studies to reduce porosity [3] and to improve hardness [7]. The strength can be increased by strong bond between the laser melted layers, higher density and reduced porosity or defects resulting in the robust microstructure.

Fig. 13(b) shows the contour plots of the maximum SP load with respect to the scan speed and energy density. The valid range of the energy density was 45-75 J/mm^3 and the possible range of the scan speed was 1200-2800 mm/s. Since the laser power was not controlled independently but determined by the energy density and the laser power conditions according to Eq. (4), the laser power range which is not available by the current SLM machine, is included in Fig. 13(b). The available laser power was 135-315 W. In Fig. 13(b), the range is shown by dashed line, in which the laser power higher than 315 W is required. In Fig. 13(b), all of the measured data points in Table 2 are also indicated.

In Fig. 6(a), the SP strength was the highest when the energy density was approximately 64.29 J/mm^3. Even though this result was obtained under the constant laser power of 180 W, it could be assumed that the energy density of 64.29 J/mm^3 as an optimal value for other laser power conditions too. In Fig. 13(b), the scan speed was 1884 mm/s (with a laser power higher than 242 W) for the energy density of 64.29 J/mm^3. This scan speed is recommended to fabricate SLM parts in the shortest time without losing material strength (1021.2 N) and without any metallurgical defect. However, as statistical point of view, it is recommended to expand the scale map by conducting the test from the block which was fabricated with other process parameters. Then, the much reliable optimized process parameters could be obtained.

4. Conclusions

An experimental study on high temperature strength of 17-4PH steel manufactured by SLM process was carried out at 425 °C using the SP tests. Effects of processing parameters such as the energy density, scan speed and laser power on microstructure and strength were investigated. The following conclusions are obtained:

(a) The higher strength which was represented by the maximum SP load, was obtained when the energy density was increased during SLM manufacturing. The SP specimen with high strength showed a fracture surface having a major circular shaped crack. The non-circular crack shape with several secondary cracks was observed in the SP specimens with low strength due to the internal defects such un-melted regions or pores.

(b) Microstructural phases verified by XRD analysis were the martensitic (α') and retained austenitic (γ) structures. The retained austenite and pore defects were increased with increase in the scan speed and with decrease in the energy density. The largest volume fraction of the retained austenite was 17.22 % when the energy density was 45.00 J/mm^3. The main factors significantly reducing the strength of the 17-4PH SLM product could be the retained austenite and pores.

(c) A RSM model was applied to investigate the effect of process parameters for obtaining the maximum SP load of 1021.2 N. The scan speed could be increased up to 1884 mm/s (with a laser power higher than 242 W) with the energy density of 64.29 J/mm^3, which is the condition recommended for fabricating the SLM parts without losing material strength and with minimum manufacturing defects.

Acknowledgments

This research was supported by Chung-Ang University Research Grants in 2020. Authors are appreciate technical support from the KMTL (Kobe Material Testing Laboratory Co).

Nomenclature

P_{SP} : Maximum small punch load
V : Scan speed
E : Energy density
a : Small punch specimen thickness
p : Laser power
d : Hatching distance
e : Layer thickness

References

[1] H. K. Rafi, D. Pal, N. Patil, T. L. Starr and B. E. Stucker, Microstructure and mechanical behavior of 17-4 precipitation hardenable steel processed by selective laser melting, *Journal of Materials Engineering and Performance*, 23 (12) (2014) 4421-4428.

[2] G. Casalino, S. L. Campanelli, N. Contuzzi and A. D. Ludovico, Experimental investigation and statistical optimisation of the selective laser melting process of a maraging steel, *Optics & Laser Technology*, 65 (2015) 151-158.

[3] N. Read, W. Wang, K. Essa and M. M. Attallah, Selective laser melting of AlSi10Mg alloy: process optimisation and mechanical properties development, *Materials & Design*, 65 (2015) 417-424.

[4] S. Pasebani, M. Ghayoor, S. Badwe, H. Irrinki and S. V. Atre, Effects of atomizing media and post processing on mechanical properties of 17-4 PH stainless steel manufactured via selective laser melting, *Additive Manufacturing*, 22 (2018) 127-137.

[5] K. N. Amato, S. M. Gaytan, L. E. Murr, E. Martinez, P. W. Shindo, J. Hernandez and F. Medina, Microstructures and mechanical behavior of Inconel 718 fabricated by selective laser melting, *Acta Materialia*, 60 (5) (2012) 2229-2239.

[6] M. J. K. Lodhi, K. M. Deen, M. C. Greenlee-Wacker and W. Haider, Additively manufactured 316L stainless steel with improved corrosion resistance and biological response for biomedical applications, *Additive Manufacturing*, 27 (2019) 8-19.

[7] H. Zhang, H. Zhu, T. Qi, Z. Hu and X. Zeng, Selective laser melting of high strength Al–Cu–Mg alloys: processing, microstructure and mechanical properties, *Materials Science and Engineering: A*, 656 (2016) 47-54.

[8] R. Li, Y. S. Kim, H. Van Tho, Y. J. Yum, W. J. Kim and S. Y. Yang, Additive manufacturing (AM) of piercing punches by the PBF method of metal 3D printing using mold steel powder materials, *Journal of Mechanical Science and Technology*, 33 (2) (2019) 809-817.

[9] G. Miranda, S. Faria, F. Bartolomeu, E. Pinto, S. Madeira, A. Mateus and O. Carvalho, Predictive models for physical and mechanical properties of 316L stainless steel produced by selective laser melting, *Materials Science and Engineering: A*, 657 (2016) 43-56.

[10] A. Yadollahi, N. Shamsaei, S. M. Thompson and D. W. Seely, Effects of process time interval and heat treatment on the mechanical and microstructural properties of direct laser deposited 316L stainless steel, *Materials Science and Engineering: A*, 644 (2015) 171-183.

[11] L. E. Murr, E. Martinez, J. Hernandez, S. Collins, K. N. Amato, S. M. Gaytan and P. W. Shindo, Microstructures and properties of 17-4 PH stainless steel fabricated by selective laser melting, *Journal of Materials Research and Technology*, 1 (3) (2012) 167-177.

[12] L. Facchini, N. Vicente, I. Lonardelli, E. Magalini, P. Robotti and A. Molinari, Metastable austenite in 17–4 precipitation - hardening stainless steel produced by selective laser melting, *Advanced Engineering Materials*, 12 (3) (2010) 184-188.

[13] A. Yadollahi, N. Shamsaei, S. M. Thompson, A. Elwany and L. Bian, Mechanical and microstructural properties of selective laser melted 17-4 PH stainless steel, *ASME 2015 International Mechanical Engineering Congress and Exposition*, American Society of Mechanical Engineers (2015).

[14] A. Yadollahi, N. Shamsaei, S. M. Thompson, A. Elwany and L. Bian, Effects of building orientation and heat treatment on fatigue behavior of selective laser melted 17-4 PH stainless steel, *International Journal of Fatigue*, 94 (2017) 218-235.

[15] D. Croccolo, M. De Agostinis, S. Fini, G. Olmi, N. Bogojevic and S. Ciric - Kostic, Effects of build orientation and thickness of allowance on the fatigue behaviour of 15–5 PH stainless steel manufactured by DMLS, *Fatigue & Fracture of Engineering Materials & Structures*, 41 (2018) 900-916.

[16] P. Edwards and M. Ramulu, Effect of build direction on the fracture toughness and fatigue crack growth in selective laser melted Ti - 6Al - 4 V, *Fatigue & Fracture of Engineering Materials & Structures*, 38 (2015) 1228-1236.

[17] Z. Hu, H. Zhu, H. Zhang and X. Zeng, Experimental investigation on selective laser melting of 17-4PH stainless steel, *Optics & Laser Technology*, 87 (2017) 17-25.

[18] H. Gu, H. Gong, D. Pal, K. Rafi, T. Starr and B. Stucker, Influences of energy density on porosity and microstructure of selective laser melted 17-4PH stainless steel, *2013 Solid Freeform Fabrication Symposium,* 474 (2013).

[19] A. A. Adeyemi, E. T. Akinlabi, R. M. Mahamood, K. O. Sanusi, S. Pityana and M. Tlotleng, Influence of laser power on microstructure of laser metal deposited 17-4 ph stainless steel, *IOP Conference Series: Materials Science and Engineering*, IOP Publishing, 225 (1) (2017).

[20] P. Ponnusamy, S. H. Masood, D. Ruan, S. Palanisamy, R. R. Rashid and O. A. Mohamed, Mechanical performance of selective laser melted 17-4 PH stainless steel under compressive loading, *Solid Freeform Fabrication 2017: Proceedings* (2017) 321-331.

[21] S. L. M. Solutions, *SLM Material Data,* www.slm-solutions.com (2012).

[22] M. P. Manahan, A. S. Argon and O. K. Harling, The development of a miniaturized disk bend test for the determination of postirradiation mechanical properties, *Journal of Nuclear Materials*, 104 (1981)1545-1550.

[23] T. Misawa, T. Adachi, M. Saito and Y. Hamaguchi, Small punch tests for evaluating ductile-brittle transition behavior of irradiated ferritic steels, *Journal of Nuclear Materials*, 150 (2) (1987) 194-202.

[24] CEN, *CWA 15627 Workshop Agreement: Small Punch Test Method for Metallic Materials*, European Committee for Standardisation (2006).

[25] Y. W. Ma and K. B. Yoon, Assessment of tensile strength using small punch test for transversely isotropic aluminum 2024 alloy produced by equal channel angular pressing, *Materials Science and Engineering: A*, 527 (16-17) (2010) 3630-3638.

[26] Z. X. Wang, H. J. Shi, J. Lu, P. Shi and X. F. Ma, Small punch testing for assessing the fracture properties of the reactor vessel steel with different thicknesses, *Nuclear Engineering and Design*, 238 (12) (2008) 3186-3193.

[27] P. Dymáček and K. Milička, Creep small-punch testing and its numerical simulations, *Materials Science and Engineering: A*, 510 (2009) 444-449.

[28] Y. W. Ma, S. Shim and K. B. Yoon, Assessment of power law

creep constants of Gr91 steel using small punch creep tests, *Fatigue & Fracture of Engineering Materials & Structures*, 32 (12) (2009) 951-960.
[29] P. B. Bacchewar, S. K. Singhal and P. M. Pandey, Statistical modelling and optimization of surface roughness in the selective laser sintering process, *Proceedings of the Institution of Mechanical Engineers, Part B: Journal of Engineering Manufacture*, 221 (1) (2007) 35-52.
[30] L. N. Carter, Selective laser melting of nickel superalloys for high temperature applications, *Doctoral Dissertation*, University of Birmingham (2013).
[31] I. I. Cuesta and J. M. Alegre, Hardening evaluation of stamped aluminium alloy components using the small punch test, *Engineering Failure Analysis*, 26 (2012) 240-246.
[32] S. P. Singh, S. Bhattacharya and D. K. Sehgal, Evaluation of high temperature mechanical strength of Cr–Mo grade steel through small punch test technique, *Engineering Failure Analysis*, 39 (2014) 207-220.
[33] D. H. Lee, Evaluation of fracture strength and material degradation for weldment of high temperature service steel using advanced small punch test, *KSME International Journal*, 18 (9) (2004) 1604-1613.
[34] W. D. Callister, *Material Science and Engineering an Introduction*, New York: John Wiley & Sons Inc. (1994).
[35] C. T. Kwok, K. I. Leong, F. T. Cheng and H. C. Man, Microstructural and corrosion characteristics of laser surface-melted plastics mold steels, *Materials Science and Engineering: A*, 357 (1-2) (2003) 94-103.
[36] R. Li, J. Liu, Y. Shi, L. Wang and W. Jiang, Balling behavior of stainless steel and nickel powder during selective laser melting process, *Journal of Advanced Manufacturing Technology*, 59 (9-12) (2012) 1025-1035.

Ho Jun Lee received his M.S. in Mechanical Engineering from Chung-Ang University. He is currently a project researcher at KEIT (Korea Evaluation Institute of Industrial Technology). His research interests are hydrogen embrittlement and associated meatallurgical damage. He is also interested in high temperature strength and other mechanical properties of additive manufactured materials.

Van Hung Dao received his M.S. and Ph.D. degrees in Mechanical Engineering from Chung-Ang University. He is currently a postdoctoral fellow at Chung-Ang University. His research interests are microstructural analysis and application of high temperature fracture mechanics to life assessment of structural material. He is extending research to behavior of additive manufactured materials.

Young Wha Ma received his Ph.D. degree in Mechanical Engineering from Chung-Ang University, Korea in 2007. After that, he worked at Georgia Institute of Technology, U.S.A. as a postdoc. Dr. Ma is currently Senior Engineer at Doosan Heavy Industries & Construction Co. His research interests are application of high temperature fracture mechanics to residual life assessment of structural materials including anisotropic materials such as gas turbine blade.

Jong Min Yu received his M.S. in Mechanical Engineering from Chung-Ang University. He is currently a Ph.D. candidate in Chung-Ang University. His research interest is life and integrity assessment of facilities in power and process plants. He is currently involved in the study on mechanical properties of additive manufactured components with various process parameters.

Kee Bong Yoon received his B.S. in Mechanical Engineering from Seoul National University, M.S. from KAIST and Ph.D. from Georgia Institute of Technology. He is currently a Professor at Chung-Ang University. His research interests are high temperature fracture and risk based management of energy plants and semiconductor plants. He has particular interest in failures of the facilities in semiconductor companies. He is extending his research to fracture of additive manufactured materials.